CORE PERFORMANCE AND MIX IN DIRECT-DRIVE SPHERICAL IMPLOSIONS ON OMEGA

C. Stoeckl,[a] J. A. Delettrez,[a] R. Epstein,[a] V. Yu. Glebov,[a] R. L. Keck,[a] R. L. McCrory,[a] P. W. McKenty,[a] F. J. Marshall,[a] D. D. Meyerhofer,[a,1] P. B. Radha,[a] S. P. Regan,[a] S. Roberts,[a] W. Seka,[a] S. Skupsky,[a] V. A. Smalyuk,[a] C. Sorce,[a] J. M. Soures,[a] R. P. J. Town,[a] B. Yaakobi,[a] J. A. Frenje,[b] C. K. Li,[b] R. D. Petrasso,[b,2] F. H. Seguin,[b] K. Fletcher,[c] S. Padalino,[c] C. Freeman,[c] N. Izumi,[d] R. Lerche,[d] T. W. Phillips,[d] and T. C. Sangster[d]

Abstract

A wide variety of diagnostics have been deployed to study direct-drive spherical implosions of gas-filled, plastic shells on the 60-beam OMEGA laser system at the Laboratory for Laser Energetics. Neutron detectors using plastic scintillators measure primary yield, ion temperature, secondary neutron yield, and burn history. Charged-particle detectors record, on CR-39 samples, the secondary protons in pure D_2 implosions and elastically scattered protons, deuterons, and tritons in DT implosions to measure the shell and fuel areal densities. Primary D^3He protons from plastic shells with a CD layer at the shell–gas interface and a ^3He fill provide a significant signal only if the shell and fuel regions are mixed. Shells with an Ar-doped fill are used to infer the emissivity-averaged core electron temperatures and densities from the measured time-dependent Ar *K*-shell spectra. The level of nonuniformity in the shell areal density at stagnation is measured using gated x-ray images of Ti-doped shells.

The application of a large number of diagnostics to these implosions significantly improves the understanding of the core conditions and fuel–shell mix.

---

[a] Laboratory for Laser Energetics, University of Rochester, Rochester, NY 14623.
[1] Also Departments of Mechanical Engineering and Physics and Astonomy, University of Rochester
[b] Plasma Science and Fusion Center, MIT
[2] Also visiting scientist, LLE.
[c] SUNY Geneseo, NY
[d] Lawrence Livermore National Laboratory

Advanced Diagnostics for Magnetic and Inertial Fusion, Edited by Stott *et al.*
Kluwer Academic/Plenum Publishers, New York, 2002

1. INTRODUCTION

In the direct-drive approach to laser-driven inertial confinement fusion (ICF)[1] a spherical target is symmetrically illuminated by a number of individual laser beams. Target and laser illumination nonuniformities are the primary determinants of implosion performance. Illumination uniformity includes both individual-beam uniformity and on-target beam-to-beam power history differences (power balance), while target nonunformities include those on both the inner and outer capsule surfaces. Nonuniformities of either kind can lead to distortions in the compressed core due to secular growth of low-order ($\ell \leq 10$) modes and shell breakup and mix due to the Rayleigh–Taylor (RT)[2,3] growth of perturbations imprinted by high-order ($\ell > 10$) nonuniformities. Ignition with direct-drive ICF relies on the generation of a "spark" in the compression "hot spot" to begin the nuclear burn process.[4] The hot spot is a high-temperature, low-density region surrounded by a low-temperature, high-density region into which the burn wave propagates, leading to significant energy gain. For an ICF target to ignite, a significant fraction of the hot spot must remain "clean," unperturbed by the evolution of the RT instability. Thus, one expects that the compressed core of a direct-drive ICF implosion will consist a central hot spot, which is mostly compressed fuel, with a region where fuel and shell materials are mixed at larger radii. This region is surrounded by cold shell material. This paper describes techniques used to study the conditions in the compressed target, including those that are more sensitive to one or more of the regions described above.

The effects of Rayleigh–Taylor instabilities on target performance have been studied on direct-drive implosions of gas-filled plastic shells on the OMEGA laser system.[5] These targets are surrogates[6] for cryogenic implosions. The stability of these shells driven with a 1-ns square laser pulse have been shown to be similar to OMEGA cryogenic targets,[7] which are energy scaled from the NIF direct-drive-ignition targets. Plastic shells are advantageous because a wide variety of shell/gas conditions and diagnostics can be applied to study various details of the implosions.[8,9] OMEGA's reproducible laser pulses give confidence to the assumption that the implosion hydrodynamics is unchanged for different target types and fill-gas makeup. Various diagnostics have been used to probe different parts of the compressed target. Primary (single-step) neutron and charged-particle yields are most sensitive to the regions of the core where fuel exists at high ion temperatures. Secondary (two-step) neutron and charged-particle yields probe both central and mix regions, depending on the temperature profile.

2. DIAGNOSTICS

2.1. Neutron and Particle Diagnostics

The primary (N_p) neutron yield is measured using quenched plastic scintillators coupled to fast photomultipliers.[10] For the range of yields recorded, the typical uncertainty in these measurements is 10%. The neutron-averaged ion temperature is

inferred from the thermal broadening of the neutron signal recorded on the detector. A convolution $m(t) = g(t) \otimes d(t)$ of a Gaussian $g(t)$ and an exponential decay $d(t)$ as is fitted to the measured signal to improve the accuracy of the ion-temperature measurement.[11] The ion-temperature-measurement uncertainty for these experiments is of the order of ~0.5 keV.

The fusion-reaction-rate history is recorded by the neutron temporal diagnostic (NTD)[12] with a time resolution of 25 ps (FWHM); NTD is based on the fast rise time of a commercially available plastic scintillator. Neutron collisions with the scintillator convert neutron kinetic energy to 350 to 450-nm-wavelength light. The light is collected and transported by an *f*/2 optical system to the photocathode of a fast streak camera, whose output image is recorded by a CCD camera. An optical fiducial system provides absolute timing with an uncertainty of ≤50 ps.

For DT-filled implosions, the fuel areal density is determined from the number of elastically scattered knock-on fuel particles:[13,14] $n + \mathrm{T(D)} \rightarrow n' + \mathrm{T'(D')}$. The shell areal density is inferred from the elastically scattered shell protons: $n + p \rightarrow n' + p'$. The yield of knock-on particles is insensitive to the electron temperature profile.[13,14]

The secondary proton $\mathrm{D} + \mathrm{D} \rightarrow {}^3\mathrm{He} + n$ followed by ${}^3\mathrm{He} + \mathrm{D} \rightarrow p(12 \sim 17\ \mathrm{MeV}) + {}^4\mathrm{He}$ and neutron $\mathrm{D} + \mathrm{D} \rightarrow \mathrm{T} + p$ followed by $\mathrm{T} + \mathrm{D} \rightarrow n(12 \sim 17\ \mathrm{MeV}) + {}^4\mathrm{He}$, yields depend on the electron temperature profile in the core and typically provide limits on the ρR_f and the core electron temperature, as well as information about the deviations in temperature and density profiles from 1-D predictions.[15,16] The areal density of the plastic shell, ρR_s, during stagnation can be inferred using the downshift of the secondary protons from D_2 implosions (produced with 12- to 17-MeV energies). The secondary protons are slowed by an amount proportional to ρR_{total}. Using the measured fuel areal density, the shell areal density can be inferred:[15] $\rho R_s = \rho R_{\mathrm{total}} - \rho R_{\mathrm{fuel}}$.

The core–fuel mix characteristics are inferred in a number of ways. The measured secondary neutron and proton yields from the shell regions can be compared to 1-D simulations. When the yields are significantly different from those predicted, they provide information about fuel–shell mix. An implosion of a plastic shell with a CD layer and a ^{3}He fill provides a significant primary D^{3}He proton signal only if the shell and fuel regions are mixed. This yield depends on the characteristics of the mix, either microscopic (diffusive) or macroscopic, where islands of shell material penetrate the core.

The secondary neutron yield is measured by the multichannel, single-hit detector MEDUSA[17] or by current-mode detectors.[18] The secondary proton and knock-on particle yields are measured with wedged range filters[15] and charged-particle spectrometers (CPS).[19] CR-39 nuclear emulsion is used in both detectors to determine the yield and the energy spectrum.

2.2. X-ray Spectroscopic Diagnostics

In some cases, the D_2 fuel is doped with 0.05 atm of Ar. This level of Ar dopant has only a small effect on the target performance. Time-resolved Ar *K*-shell spectra are recorded with a flat crystal spectrometer coupled to an x-ray streak camera with 25-ps resolution. The emissivity-averaged core electron temperature and density evolutions are inferred from the time-dependent Ar *K*-shell spectral line shapes of the Ar He-β, He-γ,

He-δ, and Ly-β resonant transitions and their associated satellites.[20] The line shapes depend strongly on the electron density and are relatively insensitive to the electron temperature, while the relative intensities are sensitive to variations in both electron temperature and density.[21] Spectral lineouts at different times are compared to a large database of synthetic spectra calculated by following Ref. 22.

2.3. X-ray Imaging

Areal-density modulations in a titanium-doped layer in the CH shell are determined from the intensity ratios of time-resolved, 2-D core images taken above and below the Ti *K* edge.[23] The 20-μm-thick shells contained an inner layer of 1.9-μm-thick CH doped with Ti (6% by atom). The initial Ti areal density in the shell is about 0.05 mg/cm^2. The emission from Ti-doped CH shells is imaged onto a four-strip framing camera[24,25] using a 6-μm-diam pinhole array, protected by a 200-μm-thick Be filter. The upper two strips of the framing camera are filtered by a 75-μm-thick Ti filter and the lower two strips by a 50-μm-thick Fe filter to image core radiation at photon energies below (~4.8 keV) and above (~6.5 keV) the Ti *K* edge (4.966 keV), simultaneously. The two x-ray energy channels have spectral bandwidths ($\Delta E/E$) of about 20%. Each image taken with the framing camera had a temporal resolution of ~40 ps and a spatial resolution of ~6 μm. The framing camera output was captured on a CCD camera with a 9-μm pixel size and a magnification of 25.

3. LASER CONDITIONS

An ~23-kJ, 1-ns square pulse delivered by the 60-beam OMEGA laser system[5] was used to drive the implosions described in this work. The beam-to-beam UV energy balance was typically ≤5% rms.[26] When beam overlap on target was included, the on-target nonuniformity due to beam-to-beam energy imbalance was <1% ($\ell \leq 12$). Individual-beam smoothing is accomplished by using smoothing by spectral dispersion (SSD),[27] distributed phase plates (DPP),[28] and polarization smoothing (PS) with birefringent wedges.[29] The two-dimensional (2-D) SSD operates at a single color cycle with 1-THz bandwidth.

4. EXPERIMENTAL RESULTS

This section reports the results of the various diagnostics described above on a series of implosions using targets with (940±30)-μm-diam, (19.5±1)-μm-thick plastic shells. Some shells have CD or titanium-doped (CHTi) internal layers. The targets are filled 15 atm of either He^3, D_2, or DT, sometimes doped with trace amounts of Ar. For the targets with pure He^3, the gas pressure is adjusted so that the hydrodynamics of the implosion, determined mostly by the electron and ion pressure, is the same. These implosions have convergence ratios (initial to final radius of the fuel–shell boundary) calculated by 1-D simulations of 15. The ratio of the measured primary neutron yield to that predicted by 1-D simulations ["yield over clean" (YOC)] for CH shells with D_2 fills

is very reproducible around 35±5%.[26] The neutron-averaged ion temperature was measured at 3.5 keV, which is about 0.5 keV higher than the 1-D predictions.

The 1-D predictions of areal density for these shells are $\rho R_f = 16$ mg/cm^2 and $\rho R_s = 60$ mg/cm^2. The total ρR as determined from the D^3He secondary protons of D_2-filled shells is found to be 76 mg/cm^2. The ρR_f inferred from the D knock-on yield is 15 mg/cm^2, while $\rho R_s \sim 61$ mg/cm^2 from the knock-on protons, both from DT-filled targets. These measurements show that the sum of fuel and shell areal densities for DT implosions is in good agreement with the total areal density independently inferred from D_2 implosions, close to those predicted from 1-D simulations.

Comparing the fusion-reaction-rate history measured by NTD with 1-D simulations gives valuable information about the accuracy of physical models used in the codes, such as laser absorption and heat transport. In particular, the timing onset of neutron production at shock convergence along with peak neutron production is very sensitive to the value of the flux-limiter.[30] Figure 1 shows a comparison between measured and predicted fusion-reaction-rate histories. A relatively minor change in the flux limiter of about 15%, from 0.06 to 0.07, leads to a significant shift in the burn history, well outside the experimental uncertainty of 50 ps

The emissivity-averaged electron temperature and density history is inferred from spectroscopic measurements of Ar-doped capsules. Figure 2 shows the evolution of the emissivity-averaged electron temperature and density during peak compression. The evolution of the continuum emission at ~3.5 keV is shown for comparison.[29] Note that the peak neutron emission occurs ~170 ps before the peak continuum emission, consistent with 1-D simulations. The measured peak electron temperature of ~2 keV is much lower than the corresponding neutron-averaged ion temperature of 3.5 keV, which indicates that the Ar emission originates from the outer, colder regions of the core and the fuel–shell mix region. The amount of fuel–pusher mixing can be inferred by combining the measurements of the fuel areal density, the core size from x-ray emission (~34 μm),

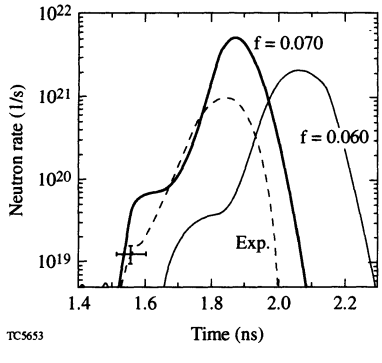

Figure 1. Comparison between measured and predicted fusion-reaction-rate histories for 20-μm shells filled with 15 atm of D_2. A relatively minor change in the flux limiter of about 15% from 0.06 to 0.07 leads to a significant shift in the burn history, well outside the experimental uncertainty of 50 ps.

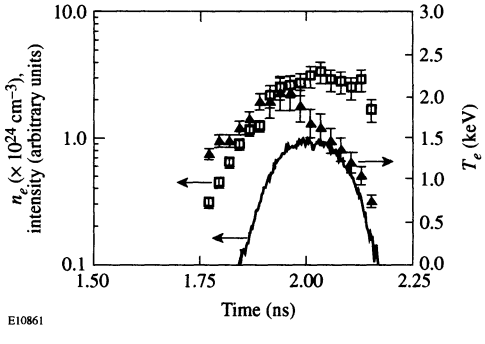

Figure 2. Temporal evolution of the emissivity-averaged core electron temperature and density near peak compression. The temporal evolution of the ~3.5-keV continuum emission is shown for comparison.

and the electron density from spectroscopic analysis. This analysis gives an average D_2 density of 4.4±1.3 g/cm^3 and a CH density of 2.6±0.8 g/cm^3, suggesting that approximately 1/3 of the core density consists of CH from the shell in the region that dominates the Ar emission. The present Ar spectroscopic data, however, provides no information about the spatial profiles in the core.

Figure 3 shows the evolution of areal-density modulations obtained by differential x-ray imaging above and below the Ti *K* edge: 1.92, 1.97, 2.02, and 2.07 ns. The spatial scale of modulations decreases from t = 1.92 ns to t = 2.02 ns (as evident from the motion of the "circular" structure in corresponding images). After that, the shorter-scale modulations start to grow, which can be seen in the image at 2.07 ns. The image size at 2.07 ns is smaller than images at early times because the level of backlighter emission drops late in the implosion. The areal-density modulations are relatively modest (18% at peak compression), indicating a shell behavior close to 1-D. The modulations decrease toward peak compression, probably due to the convergence of the target.

5. MIX MEASUREMENTS

The D^3He proton yield from a CH shell with an inner 1-mm-thick CD layer was $1.0\pm0.2 \times 10^7$ and dropped by an order of magnitude when the CD layer was offset from the inner surface of the shell by 1 μm. This indicates the presence of fuel–shell mixing during the compression. A model of the mix profiles, described in Refs. 26 and 31, indicates that approximately 50% predicted by 1-D simulations is "clean," with close-to predicted parameters.

6. SUMMARY

A wide variety of neutron, particle, and x-ray diagnostics have been deployed to study the performance of CH-shell implosions on OMEGA. The experimental observations are consistent with the picture that the compressed core at peak neutron production has an inner clean region, whereas a significant amount of shell material is mixed into the outer part of the core. The measured primary neutron yield is ~35% of that predicted from 1-D calculations. The fuel and shell areal densities determined by knock-on particles and the slowing down of secondary protons are close to their predicted values. The areal-density modulations of the shell as measured by differential x-ray imaging are below 20%, which independently indicates a shell behavior close to 1-D.

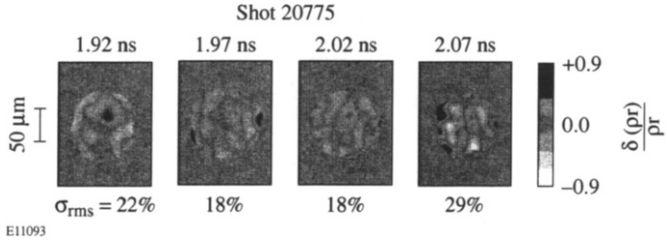

Figure 3. Evolution of areal-density modulations obtained by differential x-ray imaging.

7. ACKNOWLEDGMENTS

This work was supported by the U.S. Department of Energy Office of Inertial Confinement Fusion under Cooperative Agreement No. DE-FC03-92SF19460, the University of Rochester, and the New York State Energy Research and Development Authority. The support of DOE does not constitute an endorsement by DOE of the views expressed in this article.

8. REFERENCES

1. J. Nuckolls, L. Wood, A. Thiessen, and G. Zimmerman, Laser compression of matter to super-high densities: thermonuclear (CTR) applications, *Nature* **239**, 139–142 (1972).
2. J. D. Kilkenny, S. G. Glendinning, S. W. Haan, B. A. Hammel, J. D. Lindl, D. Munro, B. A. Remington, S. V. Weber, J. P. Knauer, and C. P. Verdon, A review of the ablative stabilization of the Rayleigh-Taylor instability in regimes relevant to inertial confinement fusion, *Phys. Plasmas* **1**(5), 1379–1389 (1994).
3. S. E. Bodner, D. G. Colombant, J. H. Gardner, R. H. Lehmberg, S. P. Obenschain, L. Phillips, A. J. Schmitt, J. D. Sethian, R. L. McCrory, W. Seka, C. P. Verdon, J. P. Knauer, B. B. Afeyan, and H. T. Powell, Direct-drive laser fusion: Status and prospects, *Phys. Plasmas* **5**(5), 1901–1918 (1998).
4. J. D. Lindl, *Inertial Confinement Fusion: The Quest for Ignition and Energy Gain Using Indirect Drive* (Springer-Verlag, New York, 1998), Chap. 6, pp. 61–82.
5. T. R. Boehly, D. L. Brown, R. S. Craxton, R. L. Keck, J. P. Knauer, J. H. Kelly, T. J. Kessler, S. A. Kumpan, S. J. Loucks, S. A. Letzring, F. J. Marshall, R. L. McCrory, S. F. B. Morse, W. Seka, J. M. Soures, and C. P. Verdon, Initial performance results of the OMEGA laser system, *Opt. Commun.* **133**, 495–506 (1997).
6. F. J. Marshall, J. A. Delettrez, R. Epstein, V. Yu. Glebov, D. R. Harding, P. W. McKenty, D. D. Meyerhofer, P. B. Radha, W. Seka, S. Skupsky, V. A. Smalyuk, J. M. Soures, C. Stoeckl, R. P. Town, B. Yaakobi, C. K. Li, F. H. Séguin, D. G. Hicks, and R. D. Petrasso, Direct-drive high-convergence-ratio implosion studies on the OMEGA laser system, *Phys. Plasmas* **7**(5), 2108–2113 (2000).
7. V. N. Goncharov, P. McKenty, S. Skupsky, R. Betti, R. L. McCrory, and C. Cherfils-Clérouin, Modeling hydrodynamic instabilities in inertial confinement fusion targets, *Phys. Plasmas* **7**(12), 5118–5139 (2000).
8. M. D. Cable, S. P. Hatchett, J. A. Caird, J. D. Kilkenny, H. N. Kornblum, S. M. Lane, C. Laumann, R. A. Lerche, T. J. Murphy, J. Murray, M. B. Nelson, D. W. Phillion, H. Powell, and D. B. Ress, Indirectly driven, high convergence inertial confinement fusion implosions, *Phys. Rev. Lett.* **73**(17), 2316–2319 (1994).
9. D. K. Bradley, J. A. Delettrez, R. Epstein, R. P. J. Town, C. P. Verdon, B. Yaakobi, S. Regan, F. J. Marshall, T. R. Boehly, J. P. Knauer, D. D. Meyerhofer, V. A. Smalyuk, W. Seka, D. A. Haynes, Jr., M. Gunderson, G. Junkel, C. F. Hooper, Jr., P. M. Bell, T. J. Ognibene, and R. A. Lerche, Measurements of core and pusher conditions in surrogate capsule implosions on the OMEGA laser system, *Phys. Plasmas* **5**(5), 1870–1879 (1998).
10. R. A. Lerche and T. J. Murphy, Geometry compensation for improving speed and efficiency of scintillator-based neutron time-of-flight detectors, *Rev. Sci. Instrum.* **63**(10), 4880–4882 (1992).
11. T. J. Murphy, R. A. Lerche, C. Bennett, and G. Howe, Ion-temperature measurement of indirectly driven implosions using a geometry-compensated neutron time-of-flight detector, *Rev. Sci. Instrum.* **66**(1), 930–932 (1995).
12. R. A. Lerche, D. W. Phillion, and G. L. Tietbohl, 25 ps neutron detector for measuring ICF-target burn history, *Rev. Sci. Instrum.* **66**(1), 933–935 (1995).
13. S. Skupsky and S. Kacenjar, Measuring fuel ρR for inertial fusion experiments using neutron elastic-scattering reactions, *J. Appl. Phys.* **52**(4), 2608–2613 (1981).
14. C. K. Li, D. G. Hicks, F. H. Séguin, J. A. Frenje, K. Green, R. D. Petrasso, D. D. Meyerhofer, J. M. Soures, V. Yu. Glebov, P. B. Radha, S. Skupsky, C. Stoeckl, S. Roberts, and T. C. Sangster, Study of direct-drive, DT gas-filled-plastic capsule implosions using nuclear diagnostics on OMEGA, submitted to *Phys. Plasmas.*

15. F. H. Séguin, C. K. Li, D. G. Hicks, J. A. Frenje, K. M. Green, R. D. Petrasso, J. M. Soures, D. D. Meyerhofer, V. Yu. Glebov, C. Stoeckl, P. B. Radha, S. Roberts, C. Sorce, T. C. Sangster, M. D. Cable, S. Padalino, and K. Fletcher, Using secondary proton spectra to study imploded D_2-filled capsules at the OMEGA laser facility, submitted to *Phys. Plasmas.*
16. H. Azechi, M. D. Cable, and R. O. Stapf, Review of secondary and tertiary reactions, and neutron scattering as diagnostic techniques for inertial confinement fusion targets, *Laser Part. Beams* **9** (1), 119–134 (1991).
17. J. P. Knauer, R. L. Kremens, M. A. Russotto, and S. Tudman, Using cosmic rays to monitor large scintillator arrays, *Rev. Sci. Instrum.* **66**(1), 926–928 (1995).
18. V. Yu. Glebov, D. D. Meyerhofer, C. Stoeckl, and J. D. Zuegel, Secondary-neutron-yield measurements by current-mode detectors, *Rev. Sci. Instrum.* **72**(1), 824–827 (2001).
19. D. G. Hicks, Charged particle spectroscopy: A new window on inertial confinement fusion, Ph.D. thesis, Massachusetts Institute of Technology, 1999.
20. S. P. Regan, J. A. Delettrez, P. A. Jaanimagi, B. Yaakobi, V. A. Smalyuk, F. J. Marshall, D. D. Meyerhofer, W. Seka, D. A. Haynes, Jr., and C. F. Hooper, Characterization of direct-drive-implosion core conditions on OMEGA with time-resolved Ar K-shell spectroscopy, submitted to *Phys. Plasmas* (2001).
21. D. A. Haynes, Jr., C. F. Hooper, Jr., R. C. Mancini, D. K. Bradley, J. Delettrez, R. Epstein, and P. A. Jaanimagi, Spectroscopic analysis of Ar-doped laser-driven implosions, *Rev. Sci. Instrum.* **66**(1), 755–757 (1995).
22. D. A. Haynes, D. T. Garber, C. F. Hooper, R. C. Mancini, Y. T. Lee, D. K. Bradley, J. Delettrez, R. Epstein, and P. A. Jaanimagi, Effects of ion dynamics and opacity on stark-broadened argon line profiles, *Phys. Rev. E* **53**(1), 1042–1050 (1996).
23. V. A. Smalyuk, B. Yaakobi, J. A. Delettrez, F. J. Marshall, D. D. Meyerhofer, S. P. Regan, and R. P. J. Town, Evolution of shell nonuniformities near peak compression of spherical implosion, submitted to *Phys. Rev. Lett.* (2001).
24. V. A. Smalyuk, T. R. Boehly, L. S. Iwan, T. J. Kessler, J. P. Knauer, F. J. Marshall, D. D. Meyerhofer, C. Stoeckl, and B. Yaakobi, Fourier-space image processing for spherical experiments on OMEGA (invited), to be published in *Rev. Sci. Instrum.*
25. C. J. Pawley and A. V. Deniz, Improved measurements of noise and resolution of x-ray framing cameras at 1–2 keV. *Rev. Sci. Instrum.* **71**(3) 1286–1295 (2000).
26. D. D. Meyerhofer, J. Delettrez, R. Epstein, V. Yu. Glebov, V. N. Goncharov, R. L. Keck, R. L. McCrory, P. W. McKenty, F. J. Marshall, P. B. Radha, S. P. Regan, S. Roberts, W. Seka, S. Skupsky, V. A. Smalyuk, C. Sorce, C. Stoeckl, J. M. Soures, R. P. J. Town, B. Yaakobi, J. D. Zuegel, J. A. Frenje, C. K. Li, R. D. Petrasso, F. H. Séguin, K. Fletcher, S. Padalino, M. R. Freeman, N. Izumi, R. A. Lerche, T. W. Phillips, and T. C. Sangster, Core performance and mix in direct-drive spherical implosions with high uniformity, *Phys. Plasmas* **8**(5), 2251–2256 (2001).
27. S. Skupsky, R. W. Short, T. Kessler, R. S. Craxton, S. Letzring, and J. M. Soures, Improved laser-beam uniformity using the angular dispersion of frequency-modulated light, *J. Appl. Phys.* **66**(8), 3456–3462 (1989).
28. T. J. Kessler, Y. Lin, J. J. Armstrong, and B. Velazquez, Phase conversion of lasers with low-loss distributed phase plates, in: *Laser Coherence Control: Technology and Applications*, edited by H. T. Powell and T. J. Kessler (SPIE, Bellingham, WA, 1993), Vol. 1870, pp. 95–104.
29. T. R. Boehly, V. A. Smalyuk, D. D. Meyerhofer, J. P. Knauer, D. K. Bradley, R. S. Craxton, M. J. Guardalben, S. Skupsky, and T. J. Kessler, Reduction of laser imprinting using polarization smoothing on a solid-state fusion laser, *J. Appl. Phys.* **85**(7), 3444–3447 (1999).
30. J. Delettrez, Thermal electron transport in direct-drive laser fusion, *Can. J. Phys.* **64**(8), 932–943 (1986).
31. P. B. Radha, V. Yu. Glebov, F. J. Marshall, D. D. Meyerhofer, S. P. Regan, W. Seka, S. Skupsky, V. A. Smalyuk, J. M. Soures, C. Stoeckl, B. Yaakobi, and R. D. Petrasso, A measurement-based picture of core conditions in OMEGA implosions, *Bull. Am. Phys. Soc.* **45**(7), 164 (2000).